Journal of Applied Physics

Genetic algorithms for the design of planar THz antenna

Cite as: J. Appl. Phys. **132**, 164502 (2022); https://doi.org/10.1063/5.0120128
Submitted: 11 August 2022 • Accepted: 06 October 2022 • Published Online: 27 October 2022
Published open access through an agreement with JISC Collections

Vanessa Fenlon, Michael Cooke, Jim Mayock, et al.

Journal of Applied Physics ARTICLE scitation.org/journal/jap

Genetic algorithms for the design of planar THz antenna

Cite as: J. Appl. Phys. **132**, 164502 (2022); doi: 10.1063/5.0120128
Submitted: 11 August 2022 · Accepted: 6 October 2022 ·
Published Online: 27 October 2022

View Online Export Citation CrossMark

Vanessa Fenlon,[1,a)] Michael Cooke,[1] Jim Mayock,[2] Andrew Gallant,[1] and Claudio Balocco[1]

AFFILIATIONS

[1]Department of Engineering, University of Durham, Durham DH1 3LE, United Kingdom
[2]Viper RF, Unit 22, Parsons Court, Welbury Way, Newton Aycliffe DL5 6ZE, United Kingdom

Note: This paper is part of the Special Collection Recognizing Women in Applied Physics.
[a)]**Author to whom correspondence should be addressed:** vanessa.j.fenlon@durham.ac.uk

ABSTRACT

This paper proposes a genetic algorithm for the design of passive components operating at THz frequencies and its experimental validation using an exemplar patch antenna. The patch antenna is based on an SU8 substrate, with a binary array describing the placement of metal "bits" replacing the conventional patch. These "bits" are constrained at $25 \times 25\,\mu\text{m}^2$, ensuring ease of fabrication. Optimal configurations of this array are determined using a finite-difference time-domain solver coupled to the genetic algorithm, which simulates and optimizes for maximum power collection in the frequency range of 0.10–5.0 THz. The aim was to produce an evolved patch antenna design with double the power collection efficiency across the majority of the frequency range compared to a reference, plain patch antenna of the same size. This was successful with a 5.3 dB mean improvement in simulated power collection compared to a plain reference patch. A vector network analyzer in conjunction with 0.80–1.0 THz frequency extenders was used to validate the simulation results. The antennas were arranged in pairs with variable feed length to determine the feedline attenuation and validate the simulated antenna directionality.

I. INTRODUCTION

Spectrum scarcity is causing communications engineers to investigate previously unexplored regions of the spectrum, such as infrared and mm-wave. Research into components in the unlicensed wireless band at 60 GHz is ongoing, with approximately 7 GHz of bandwidth available.[1] This provides an acceptable solution for high-definition media transfer.[2] However, it is expected that data rates above 100 Gbps will be achieved using frequencies above 100 GHz.[3] The THz gap (0.1–10 THz[4]) is increasingly being scouted for 6G potential,[5] with speeds of up to 46 Gbps demonstrated for wireless communications at 0.4 THz.

The THz frequency range poses unique challenges, including high water-vapor attenuation[6] and the need for micro-scale components, which can limit the achievable power transfer. THz components, including broadband antennas, such as those described in this paper, therefore, need to be highly optimized for power efficiency to compensate for this.

The optimization of passive THz components, such as filters and antennas, is typically based on the well-established numerical methodologies developed for microwave frequencies. However, these methods are not well-suited for optimization against a target performance (e.g., power efficiency) at THz frequencies, as they tend to result in more complex geometries that cannot be readily realized at the micrometer scale. For this, bespoke optimization tools would be of benefit. Genetic algorithms (GAs) have been successful at developing new devices and antennas at MHz and GHz frequencies,[7,8] but their use in THz component design is still largely unexplored.

Compared to other numerical methods, GAs are more likely to scale well to THz frequencies because they can optimize within many constraints at once. The challenge of manufacturing at the micrometer scale can be avoided by specifying constraints, such as minimum feature size. Another advantage of GAs is that they can optimize over a wide band of frequencies concurrently, which is difficult to achieve using conventional design techniques.

GAs use Darwinian evolution as a metaheuristic computational technique to find optimized solutions to a variety of problems. The algorithm is initialized with a collection (or *population*) of designs (referred to as *individuals*), represented by a vector (the *genome*), which contains all the required parameters (the *chromosomes*). The initial population is often randomly generated. The individuals are subject to selection through a fitness test; the fittest individuals are used to create another generation using *genetic reproduction*. This is an iterative process where the individuals of each generation are used as the *parents* for the next (*progeny*). The algorithm is terminated at a set fitness level, number of generations, or after maximum fitness stagnation.[9] The best output is normally called an *evolved* result or device. These algorithms can be written to evolve the shape of components to maximize a specific fitness function, which describes the desired component behavior.

In this paper, we present a GA that can be used to optimize a variety of passive components, such as filters, circulators, and impedance matching networks.[10,11] This GA is available online and free to use.[12]

Here, it has been utilized to optimize the power collection efficiency of a patch antenna while also constraining the design for manufacturability. The capability of the GA to optimize over a very large bandwidth of 0.1–5.0 THz is assessed.

This frequency range is not only important for detectors and communication devices, but also in thermal energy harvesting, where the majority of radiant heat is in the terahertz range.[13] The frequency range 0.1–5.0 THz provides a good test case for both this and evaluating the performance of the algorithm under the most demanding circumstances. As the quantum cutoff of thermal radiation at room temperature is approximately 6 THz, the far infrared and terahertz regions are ideal locations to harvest low-grade waste heat. To maximize the potential energy harvested, antennas need to be as broadband as possible.

The aim was to produce an evolved patch antenna design with double the power collection efficiency in over 50% frequency range compared to a reference, plain patch antenna of the same size.

This article is organized as follows: Sec. II details the implementation of the proposed GA. Section III presents the top-performing antenna, its fabrication process, and testing setup. Section IV reports on the experimental results and their comparison with numerical simulations.

II. ANTENNA DESIGN OPTIMIZATION

The patch antenna[14] consists of a dielectric layer sandwiched between a flat metallic ground plane and a "patch" of metal. Conventionally, the patch is continuous, but this limits the performance of the antenna to narrow-band operation. By creating apertures in the patch, the antenna bandwidth can be extended, and its impedance tailored. This technique has been used before, such as by Islam *et al.*[15] This paper investigates the viability in using genetic algorithms to design the location of these apertures.

A patch antenna with metal patch measuring $500 \times 500\,\mu\text{m}^2$ was considered. A GA was designed to optimize the power collection performance of this antenna between 0.1 and 5.0 THz by determining the optimum location of apertures within the metal patch.

An overview of the operation of the GA is shown in Fig. 1. For the simulation, the metal patch was divided into a 20×20 grid of $25\,\mu$m squares, each of which corresponded to a potential aperture location. This sets a minimum feature size of $25\,\mu$m, which was chosen for ease of fabrication. The GA operated on a two-dimensional array of binary elements, where "1" represented a region filled with metal and "0" represented an aperture. This array formed the antenna genome.

A. Initialization

The initial generation consisted of 59 randomly generated antenna designs and one reference design. The reference was a plain patch with no apertures and was used as the baseline against which to measure the performance of the evolved designs. Antenna designs were constrained to be symmetrical about the x axis to ensure a symmetric radiation pattern and reduce computational effort.

The combined population size of 60 was maintained throughout the evolution. Through testing a range of population sizes, it was found that, with a constant size of 60, the GA was unlikely to prematurely converge on a local maximum (as is a characteristic of a population that is too small) or never converge at all (as is seen in populations that are too large).

B. Finite-difference time-domain simulation

The antenna designs were simulated using a Durham-developed finite-difference time-domain (FDTD) simulator, Lucifer,[16] based on Yee's original algorithm.[17,18]

A cubic mesh with $5\,\mu$m sides was used across the domain. The domain was $2500 \times 2500 \times 100\,\mu\text{m}^3$ (x, y, z). The substrate and ground layers reached the edges of the x and y domain, as seen in the top left of Fig. 1. The metal thickness was one cell (i.e., $5\,\mu$m), and the metal was modeled by using a large negative dielectric constant ($\varepsilon_r = -1\,000\,000$).[16] A microstrip feedline of width $20\,\mu$m connected the patch to the edge of the domain. Periodic boundary conditions were used on the vertical faces, and first-order absorbing boundary conditions were used on the top and bottom faces to avoid spurious reflections.

In the simulations, the antenna was "illuminated" by a 0.78 ps pulse, shaped to the first derivative of a Gaussian function and linearly polarized along the x axis. The source was located above the antenna and directed along the z axis. The simulated time was 30 ps to accommodate one cycle at 0.1 THz.

A frequency-independent dielectric constant of 3.43 was used to represent the intended use of SU8 as the dielectric layer material.[19] SU8 was chosen because of its ease of manufacture and relatively low dielectric losses at THz frequencies.[20]

C. Fitness test

The fitness test was intended to evaluate the performance of the antenna as a broadband power receiver (without a specific frequency response). As such, the fitness test measured the overall power collection efficiency of the antenna between 0.1 and 5.0 THz by evaluating the power spectral density received in the feedline compared to that of the input.

Potential difference, in volts, is calculated as

$$V = \int_{d_1}^{d_2} E\, dl. \tag{1}$$

This is calculated from the electric field, E, transmitted along the feedline. The feedline had a length of $200\,\mu$m (external to the

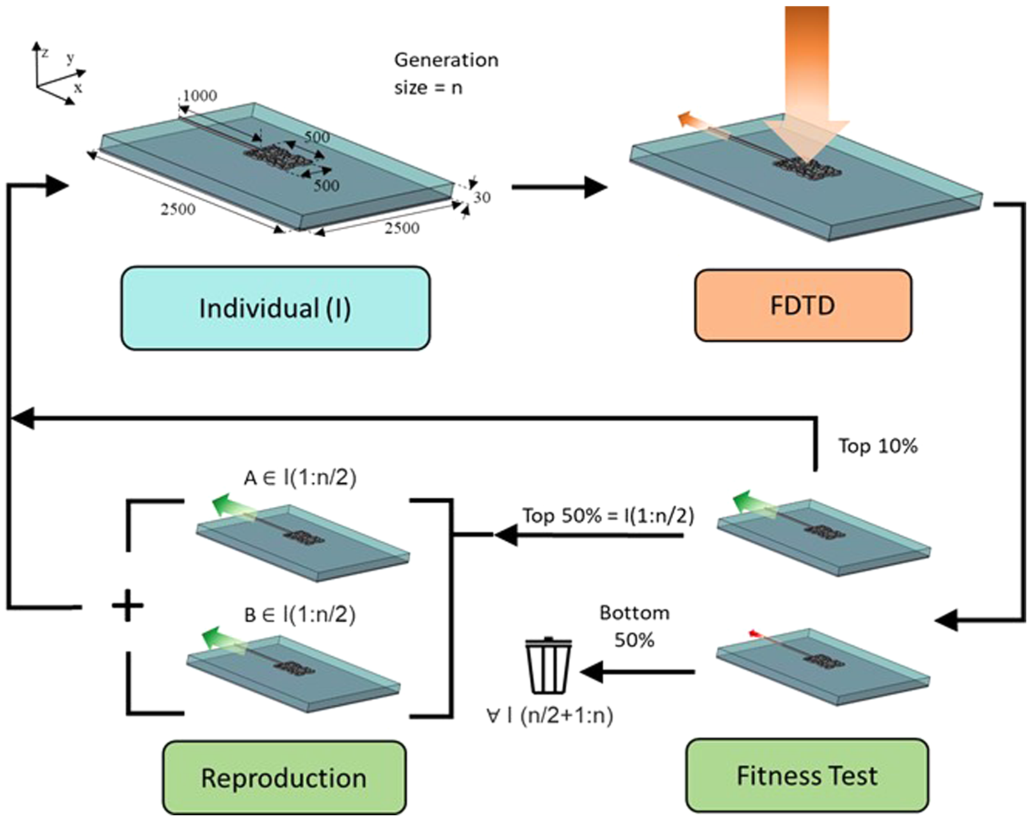

FIG. 1. Simplified genetic algorithm methodology. A patch antenna with substrate in blue modeled as an SU8 layer and metal in dark gray modeled as a perfect conductor. All dimensions are shown in micrometers.

antenna). The potential difference is calculated between locations d_1 and d_2 that are 100 and 105 μm away from the antenna, respectively.

The power spectral density (in W/Hz) of V is

$$PSD = \frac{|FFT(V)|^2}{Z_0}, \tag{2}$$

where Z_0 is the characteristic impedance of the feedline. Using the SU8 substrate's dielectric constant and thickness (30 μm) and assuming TEM transmission in the microstrip, the impedance was calculated as 96.97 Ω.[21] Before performing the FFT, the time-domain data were weighted by a Kaiser window (with β = 8) to prevent Gibb's oscillations in the spectrum.

Power efficiency (P_{eff}) was used as the fitness score and was calculated by normalizing the *PSD* over the input,

$$P_{eff} = \int_{f_1}^{f_2} \frac{PSD}{PSD_{in}}\, df, \tag{3}$$

where PSD_{in} is the power spectral density of the input pulse, $f_1 = 0.1$ THz, and $f_2 = 5.0$ THz are the lower and upper frequency limits, respectively. Individuals with a higher efficiency, therefore, received a greater fitness score and were ranked more favorably within the generation.

D. Genetic reproduction

Genetic reproduction was performed in MATLAB and consisted of three operators: *cloning*, *crossover*, and *mutation*. Cloning was the duplication of an individual so that the progeny has the same chromosomes as the single parent. Crossover combined two parents to produce a single progeny. This was implemented as in Bremermann *et al.*,[22] where each chromosome (bit) within the genome is considered in isolation. Each progeny chromosome is selected independently with equal probability from either parent's corresponding chromosome. Mutation applies random changes to the genome of a single parent to produce one new individual. The mutation algorithm was implemented by inverting a small number of chromosomes within the parent genome. Each bit had a 5% probability of being inverted.

These three operators were used to create progeny from parents as follows:

(1) The best 10% of individuals were carried through to the next generation unaltered (cloned); this ensured that there was never a decrease in the fitness score between generations.

(2) The top 50% underwent crossover and mutation to produce new antenna designs, combining favorable characteristics from well-performing individuals. These accounted for 85% of the next generation. When the simulation started to converge, as detected by a decrease in the range of fitness scores, the ratio of progeny produced by mutation compared to that produced by crossover was increased. This reduced the probability of premature convergence on local maxima by producing *radical* offspring. These are individuals with a previously unseen set of chromosomes, which would be unlikely to occur through crossover.
(3) A small, random sample of individuals from across the whole parent generation (including the bottom 50%) underwent crossover to produce the remaining 5% of the progeny; this maintained design variation, further guarding against premature convergence.

III. FABRICATION AND EXPERIMENTAL SETUP

An optimized patch antenna evolved using our algorithm is shown in Fig. 2(a) and the fabricated prototype in Fig. 2(b). A 2′ borosilicate glass substrate was coated with a 100 nm-thick aluminum ground plane using electron-beam vapor deposition. A SU8 layer with a nominal thickness of 30 μm was then spin coated onto the ground plane. The measured average thickness across the glass substrate was 32.8 μm, with a standard deviation of 7.8 μm. The patches were then defined using a photolithographic process: a 100 nm-thick aluminum layer was covered with photoresist, exposed through a mask, developed, and finally etched using H_3PO_4:HNO_3 in a 100:6 volume ratio for 45 s.

The experimental setup for measuring the antenna response is shown in Fig. 3. The experiment used a vector network analyzer (VNA) with two bidirectional VDI WR 1.0 frequency extenders for operation between 0.75 and 1.10 THz. The frequency extenders were fitted with horn antennas with a 26 dB gain.[23]

The VNA and extender heads were calibrated independently. The VNA was calibrated using an electronic calibration kit (HP 85033C). The extender heads were calibrated with a short, open, load through (SOLT) method with a VDI WR 1.0 Calibration Kit. The calibration plane is at the extender flange where the antenna is mounted, with an expected uncertainty of approximately 0.5 dB for transmission parameters.[24]

With reference to Fig. 3, port P1 transmitted to mirror M1, which focused the signal onto antenna A1 (blue beam path). A microstrip transferred the received signal to antenna A2, which re-transmitted the signal. Antennas A1 and A2 were identical. The re-transmitted signal was collimated and focused by the mirror pair M2–M3 onto port P2 (red beam path). The frequency response of the system between P1 and P2 was measured.

Multiple antenna pairs with varying lengths of connecting microstrips were tested so that losses due to the interconnection could be accounted for.

The experimental frequency range, 0.8–1.0 THz, corresponds to a wavelength range of 300–375 μm. In this region, non-line-of-sight reflections are unlikely to cause spurious features. The alignment process is designed to reduce the potentially significant diffractions caused by quasi-optics. We chose a 90° arrangement with the extender's antennas offset in the vertical direction as shown in Fig. 3 as this reduced the likelihood of spurious features caused by diffraction.

The same experimental setup was used to estimate the radiation pattern of the antennas. An aluminum sheet with a

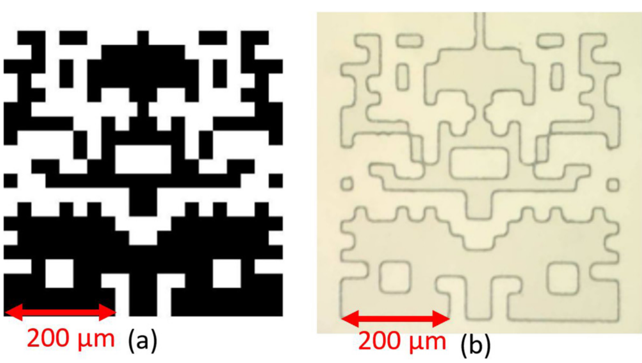

FIG. 2. Antenna pattern (a) used in simulation and (b) microphotograph of a manufactured antenna.

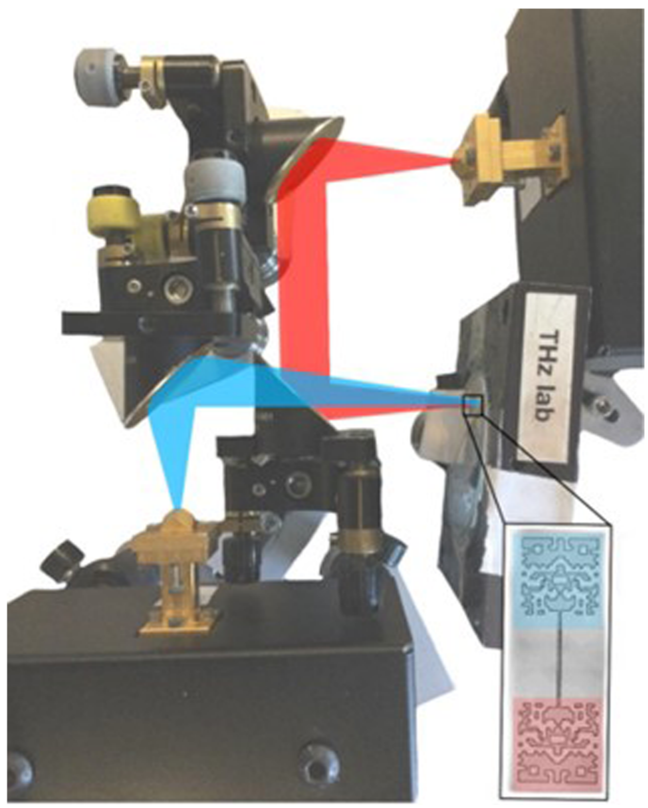

FIG. 3. Antenna testing. Antennas are orientated vertically (into the page). The blue trace shows the (upper) transmission path from port P1 to antenna A1. The red trace shows the (lower) transmission path from antenna A2 to port P2.

5 mm-wide slit was placed on a linear stage. The slit was traversed incrementally across the beam path between antenna A2 and mirror M2, while the power received at port P2 was measured. The lateral offset of the slit was then converted into an angle to estimate the radiation pattern of the antenna.

IV. RESULTS

A. Genetic algorithm convergence

The convergence of the GA used to generate the antenna design in Fig. 2 is shown in Fig. 4. Note that the reference patch described in Sec. II A accounts for the best-performing antenna in the first generation.

The GA converged in only 50 generations, which is relatively fast compared to other similar algorithms and followed a typical convergence pattern.[25,26] The initial convergence was fast but followed by increasingly slow improvements. The algorithm was terminated when the generational improvement was low, as further improvements were comparatively costly. The final, best-performing antenna design showed a 290% improvement in fitness between 0.1 and 5.0 THz compared to the reference antenna.

Figure 5(a) shows the plain reference patch antenna that is the best-performing design in the first generation. There is a substantial difference between Figs. 5(a) and 5(b), where the best-performing designs are selected from predominantly randomly generated populations. As designs undergo mutation or crossover, the degree of randomness in the population decreases. Therefore, Figs. 5(c)–5(f) show smaller variations. However, these smaller design changes, such as those observed between Figs. 5(c) and 5(d), can lead to a significant improvement in the fitness score.

B. Simulation of an evolved antenna design

The simulated transmission spectrum of the reference antenna and the final best-performing evolved antenna is shown in Fig. 6. The frequency extender full range was 0.75–1.10 THz. However, the VNA experienced decreased accuracy at the extremes of this range. Figure 6(b) is plotted between 0.80 and 1.00 THz for comparison with experimental results.

Both the reference and evolved antennas were resimulated for a longer time (100 ps). This was to establish the power spectra at a sufficiently high resolution, especially at lower frequencies, to compare with measurements obtained experimentally. This also enabled the fitness improvement seen in Fig. 4 to be quantified in terms of power collection efficiency.

Figure 6(a) shows a mean improvement of 5.3 dB between 0.1 and 5.0 THz, which meets the target (set out in Sec. I) of doubling the power collection efficiency across this range. Approximately 79% of the spectrum above showed some improvement. Power collection efficiency was doubled in at least 70% of the spectrum and quadrupled in approximately half the spectrum. In addition, the largest improvement seen was 18.5 dB at 4.63 THz.

This uniform improvement shows that the algorithm converged at an optimal rate. The final, evolved solution was found quickly, but premature convergence was avoided by escaping local maxima (see Sec. II D), as evidenced by the absence of narrow, localized peaks. Both the reference and evolved antennas were experimentally verified between 0.8 and 1.0 THz in Sec. IV C. This experimental region is highlighted on the spectrum in Fig. 6(a) and plotted in full in Fig. 6(b).

C. Experimental measurements

The comparison between the measured response of the reference patch and the evolved antenna is shown in Fig. 7.

The scattering matrix, S, quantifies how power propagates through a multi-port network. For the two-port network used here

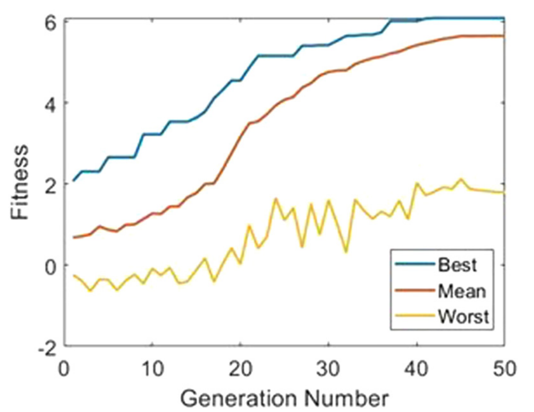

FIG. 4. Genetic algorithm fitness variation until stabilization at 50 generations. The fitness score is measured in arbitrary units. The reference antenna has fitness (F) = 2.1, which is the best of the first generation.

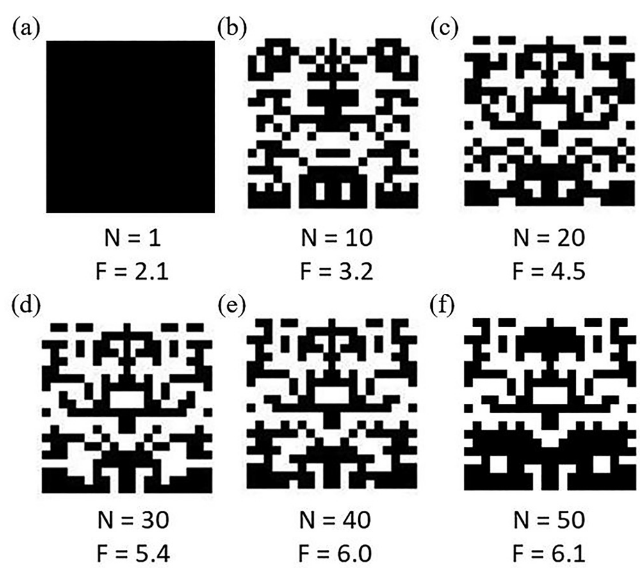

FIG. 5. Evolution of the best-performing patch antenna every ten generations. The best design from generation 1 (a), (b) 10, (c) 20, (d) 30, (e) 40, and (f) 50. N is the generation number and F the fitness score.

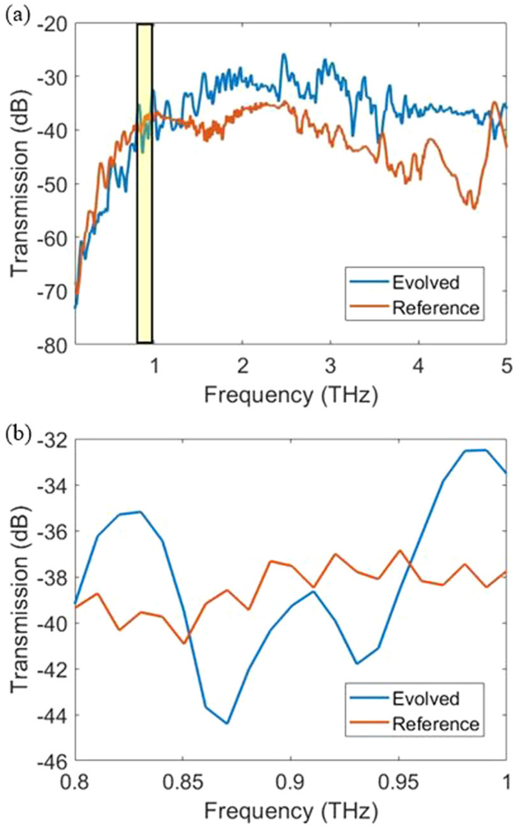

FIG. 6. Simulated spectra of the best evolved antenna after 50 generations and a filled plain reference patch from the first generation: (a) from 0.1 to 5.0 THz and (b) from 0.8 to 1.0 THz.

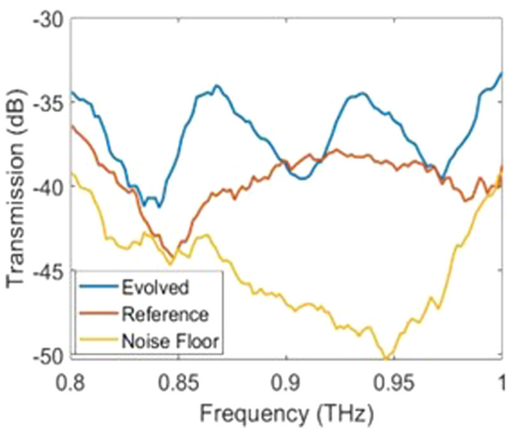

FIG. 7. Experimental results from manufactured evolved and reference patch antennas.

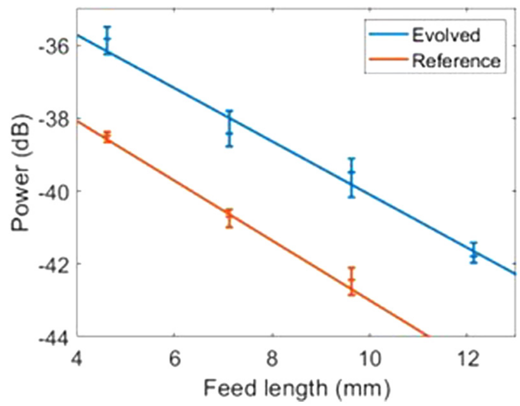

FIG. 8. Feedline characterization calculated from scattering parameter s_{21} using antenna pairs with varying lengths of microstrips between them.

(pictured in Fig. 3), there are four scattering parameters in this matrix. Parameters s_{11} and s_{22} describe the reflection into ports P1 and P2, respectively. The transmission between ports can be calculated with either s_{21} (i.e., port P1 was the source and port P2 the receiver) and s_{12} (i.e., port P2 was the source and port P1 the receiver). In Fig. 7, the transmission, T, was determined from the modulus scattering parameters: $T = |s_{21}|^2 \cong |s_{12}|^2$. The transmission, calculated with either, showed very good agreement. A ten-point moving average was applied to the data shown in Fig. 7 to smooth local peaks due to noise.

Figures 6(b) and 7 show comparable levels of transmission for each antenna type, respectively. The variations in the spectrum were expected due to the variations in antenna fabrication (slight curving of corners due to an etching process). The small frequency shift is likely due to changes in the SU8 thickness between fabricated and simulated antennas. As such, it can be concluded that the simulation and experimental results show good agreement.

Microstrips of different lengths were used to connect antenna pairs to allow for the characterization of the microstrip losses, as seen in Fig. 8.

The loss calculated from the gradients in Fig. 8 was 0.79 ± 0.06 dB/mm, which shows excellent agreement between the reference and evolved samples and promisingly low loss in both cases. For comparison, state-of-the-art gold-plated TE01 waveguides have losses ranging from 0.13 dB/mm at 0.75 THz to 0.088 dB/mm at 1.10 THz.[27] However, these waveguides require precision manufacturing and cannot be easily integrated. The microstrip presented here added no extra cost and required no dedicated process for its integration. The relatively low loss of the feedline compared to the system gain implies that the measured transmission shown in Fig. 7 is almost entirely a function of the antennas.

D. Comparison of simulated and experimental measured angular dependence

The simulated radiation pattern and measured angular dependence are shown in Fig. 9. Two frequencies are shown, 0.85 and

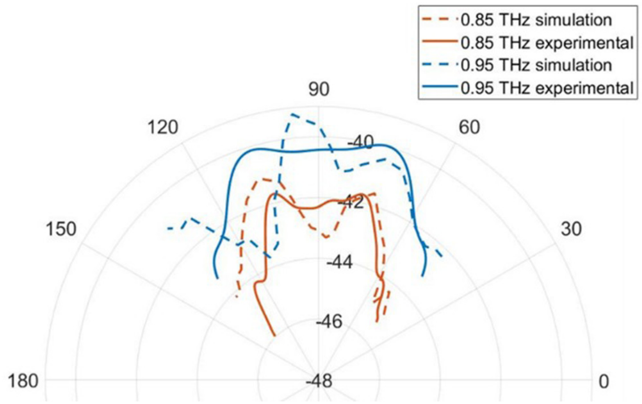

FIG. 9. Radiation patterns of evolved antennas at 0.85 and 0.95 THz. The solid line shows measured angular dependence experimentally examined through movement of a 5.0 mm slit. The dotted line shows the radiation pattern simulated using a MATLAB's antenna toolbox.

0.95 THz. The radiation pattern was simulated using a MATLAB's antenna toolbox (with adjustments for THz frequency simulations). All patterns were plotted from 45° to 135° as this was the maximum range allowed by our experimental setup described in Sec. III.

To allow simulation and measured patterns to be plotted on the same axis, the simulated radiation pattern has been shifted in magnitude to account for path losses obtained in the experiment. Figure 9 shows that the simulated radiation pattern and measured angular dependence have similar trends at 0.85 and 0.95 THz. This agreement provides evidence that the antenna's performance over the entire simulated frequency range would be reproducible experimentally.

These results support the mean improvement of 5.3 dB seen in the GA over the optimized region, 0.1–5.0 THz. As the GA improved 94% of the spectrum within this range, it can be concluded that this algorithm would be a good candidate for creating future antenna designs, with bandwidths within this region.

V. CONCLUSIONS

A genetic algorithm designed to produce a range of passive components has been presented. A broadband (0.1–5.0 THz) patch antenna optimized using this genetic algorithm showed a 290% improvement in the fitness test against a reference plain patch antenna.

The candidate antenna design was simulated for 100 ps, where the increase in the fitness score was found to correspond to a 5.3 dB mean improvement in the power collection efficiency between 0.1 and 5.0 THz. Additionally, 70% of the spectrum showed at least doubling in the efficiency compared to the reference patch.

The evolved antenna was fabricated and tested using a VNA in the 0.8–1.0 THz range, which displayed good agreement between simulated and experimental results. This success over an arbitrarily large frequency range shows that this algorithm is a good candidate for producing future antenna designs optimized for power collection at bandwidths within this region.

ACKNOWLEDGMENTS

This project is funded by the European Regional Development Fund (ERDF) (Grant No. 25R17P01847) and the Intensive Industrial Innovation Programme—North East (IIIP-NE) in collaboration with Viper RF Ltd.

AUTHOR DECLARATIONS

Conflict of Interest

The authors have no conflicts to disclose.

Author Contributions

Vanessa Fenlon: Conceptualization (equal); Data curation (equal); Formal analysis (equal); Methodology (equal); Software (equal); Writing – original draft (equal); Writing – review & editing (equal). **Michael Cooke:** Methodology (equal); Validation (equal). **Jim Mayock:** Conceptualization (equal); Supervision (equal). **Andrew Gallant:** Conceptualization (equal); Data curation (equal); Methodology (equal); Supervision (equal); Writing – review & editing (equal). **Claudio Balocco:** Conceptualization (equal); Data curation (equal); Methodology (equal); Supervision (equal); Writing – review & editing (equal).

DATA AVAILABILITY

The data that support the findings of this study are available from the corresponding author upon reasonable request.

REFERENCES

[1]Technical Specification Group Radio Access Network, "Study on scenarios and requirements for next generation access technologies" (Release 15), Technical Report No. 38.913, Version 15.0.0, 3GPP, 2018.
[2]T. S. Rappaport, J. N. Murdock, and F. Gutierrez, "State of the art in 60-GHz integrated circuits and systems for wireless communications," Proc. IEEE **99**(8), 1390–1436 (2011).
[3]T. S. Rappaport, Y. Xing, O. Kanhere, S. Ju, A. Madanayake, S. Mandal, A. Alkhateeb, and G. C. Trichopoulos, "Wireless communications and applications above 100 GHz: Opportunities and challenges for 6G and beyond," IEEE Access **7**, 78729–78757 (2019).
[4]I. Akyildiz, J. Jornet, and C. Han, "TeraNets: Ultrabroadband communication networks in the terahertz band," IEEE Wirel. Commun. **21**(4), 130–135 (2014).
[5]X. Wang *et al.*, "Millimeter wave communication: A comprehensive survey," IEEE Commun. Surv. Tutor. **20**(3), 1616–1653 (2018).
[6]M. Van Exter, C. Fattinger, and D. Grischkowsky, "Terahertz time-domain spectroscopy of water vapor," Opt. Lett. **14**(20), 1128–1130 (1989).
[7]G. Hornby, A. Globus, D. S. Linden, and J. D. Lohn, "Automated antenna design with evolutionary algorithms," in *AIAA Space* (AIAA, 2006), pp. 19–21.
[8]S. C. Panagiotou, S. C. A. Thomopoulos, T. Christos, and N. Capsalis, "Genetic algorithms in antennas and smart antennas design overview: Two novel antenna systems for Triband GNSS applications and a circular switched parasitic array for WiMAX applications developments with the use of genetic algorithms," Int. J. Antennas Propag. **2014**, 1–13.
[9]G. C. Onwubolu and B. V. Babu, *New Optimization Techniques in Engineering* (Springer, 2013), Vol. 141.

[10]J. McCubbin, V. J. Fenlon, and C. Balocco, "Impedance matching networks designed by evolutionary algorithms," in *44th IRMMW-THz* (IEEE, 2019).
[11]V. J. Fenlon *et al.*, "Genetic algorithms for the design of THz components," in *45th IRMMW-THz* (IEEE, 2020).
[12]V. Fenlon, "Agenoria Genetic Algorithm"; see https://github.com/claudiobalocco/agenoria.
[13]Y. Pan, C. V. Powell, A. M. Song, and C. Balocco, "Micro rectennas: Brownian ratchets for thermal-energy harvesting," Appl. Phys. Lett. **105**(25), 253901 (2014).
[14]J. Howell, "Microstrip antennas," IEEE Trans. Antennas Propag. **23**(1), 90–93 (1975).
[15]M. T. Islam, M. N. Shakib, and N. Misran, "Multi-slotted microstrip patch antenna for wireless communication," Prog. Electromagn. Res. Lett. **10**, 11–18 (2009).
[16]C. Balocco, "Lucifer FDTD Simulation"; see https://github.com/claudiobalocco/lucifer.
[17]K. Yee, "Numerical solution of initial boundary value problems involving Maxwell's equations in isotropic media," IEEE Trans. Antennas Propag. **14**(3), 302–307 (1966).
[18]A. Taflove, Allen, and S. C. Hagnes, *Computational Electrodynamics: the Finite-Difference Time-Domain Method* (Artech house, 2005).
[19]M. Naftaly and R. E. Miles, "Terahertz time-domain spectroscopy for material characterization," Proc. IEEE **95**(8), 1658–1665 (2007).
[20]C. Lin, C. Chang, Y. T. Cheng, and C. F. Jou, "Development of a flexible SU-8/PDMS-based antenna," IEEE Antennas Wir. Propag. Lett. **10**, 1108–1111 (2011).
[21]R. E. Collin, *Foundations for Microwave Engineering* (IEEE Press, New York, 2001).
[22]H. J. Bremermann, M. Rogson, and S. Salaff, "Global properties of evolution processes," in *Natural Automata Useful Simulations* (Spartan Books, 1966), pp. 3–41.
[23]Virgina Diodes, Inc., "Nominal Horn Specifications"; see https://www.vadiodes.com/images/AppNotes/VDI_Feedhorn_Summary_2020.05.04.pdf.
[24]N. M. Ridler and R. G. Clarke, "Establishing traceability to the International System of Units for scattering parameter measurements from 750 GHz to 1.1 THz," IEEE Trans. Terahertz Sci. Technol. **6**(1), 2–11 (2016).
[25]F. Boschetti, M. C. Dentith, and R. D. List, "Inversion of seismic refraction data using genetic algorithms," Geophysics **61**(6), 1715–1727, (1996).
[26]V. K. Koumousis and C. P. Katsaras, "A saw-tooth genetic algorithm combining the effects of variable population size and reinitialization to enhance performance," IEEE Trans. Evol. Comput. **10**(1), 19–28 (2006).
[27]Virginia Diodes, Inc., "VDI Waveguide Designations 2015.01—WR—Frequency Multipliers (WR and D Series)," (2015); see https://www.datasheetarchive.com/whats_new/22268e039b1aae10e3d7023d710573a9.html.